REEP3 and REEP4 determine the tubular morphology of the endoplasmic reticulum during mitosis

Darshan Kumar[a,†], Banafsheh Golchoubian[b,†], Ilya Belevich[a,c], Eija Jokitalo[a,c,*], and Anne-Lore Schlaitz[b,*]

[a]Cell and Molecular Biology Program and [c]Electron Microscopy Unit, Institute of Biotechnology, University of Helsinki, FI-00014 Helsinki, Finland; [b]Center for Molecular Biology of Heidelberg University (ZMBH), D-69120 Heidelberg, Germany

ABSTRACT **The endoplasmic reticulum (ER) is extensively remodeled during metazoan open mitosis. However, whether the ER becomes more tubular or more cisternal during mitosis is controversial, and dedicated factors governing the morphology of the mitotic ER have remained elusive. Here, we describe the ER membrane proteins REEP3 and REEP4 as major determinants of ER morphology in metaphase cells. REEP3/4 are specifically required for generating the high-curvature morphology of mitotic ER and promote ER tubulation through their reticulon homology domains (RHDs). This ER-shaping activity of REEP3/4 is distinct from their previously described function to clear ER from metaphase chromatin. We further show that related REEP proteins do not contribute to mitotic ER shaping and provide evidence that the REEP3/4 carboxyterminus mediates regulation of the proteins. These findings confirm that ER converts to higher curvature during mitosis, identify REEP3/4 as specific and crucial morphogenic factors mediating ER tubulation during mitosis, and define the first cell cycle-specific role for RHD proteins.**

Monitoring Editor
Anne Spang
University of Basel

Received: Nov 2, 2018
Revised: Mar 18, 2019
Accepted: Apr 10, 2019

INTRODUCTION

The endoplasmic reticulum (ER) is a single membrane network of high curvature tubules and flat cisternae with highly curved edges, called ER sheets (Shibata *et al.*, 2006; Goyal and Blackstone, 2013).

A major structural determinant of ER tubules and the curved edges of ER sheets are morphogenic proteins containing reticulon homology domains (RHDs), in particular Reticulons (RTN1-4 in mammals) and REEP proteins (REEP1-6 in mammals). RHDs consist of paired hydrophobic hairpin structures that are believed to stabilize high membrane curvature by acting as wedges in the cytoplasmic leaflet of the ER membrane and by oligomerizing into scaffolds (Voeltz *et al.*, 2006; Shibata *et al.*, 2010; Westrate *et al.*, 2015). During interphase, the peripheral ER and the nuclear envelope (NE) are two connected subdomains of the organelle. As cells enter mitosis, the NE disassembles and its membrane-associated components disperse across the peripheral ER. Throughout mitosis, the peripheral ER remains a single network and retracts from chromatin (Ellenberg *et al.*, 1997). After chromosome segregation, ER contacts daughter cell chromatin to initiate the formation of a new NE (Güttinger *et al.*, 2009; Schellhaus *et al.*, 2016). Thus, ER morphology and dynamics are tightly coupled to NE dynamics during mitosis. In addition, the ER has been proposed to contribute to cytokinesis and may serve as a "spindle envelope" that promotes mitotic spindle assembly (Prekeris and Gould, 2008; Zhang *et al.*, 2010; Schweizer *et al.*, 2015). Hence, it is likely that the ER is remodeled at the onset of mitosis to fulfill a variety of cell cycle-specific functions. However,

This article was published online ahead of print in MBoC in Press (http://www.molbiolcell.org/cgi/doi/10.1091/mbc.E18-11-0698) on April 17, 2019.

The authors declare that they have no conflict of interest.

[†]These authors contributed equally to this work.

Author contributions: A.S. and E.J. designed the study and acquired funding. D.K., B.G., I.B., and A.S. performed experiments. A.S. wrote the paper. All authors contributed to data analysis and data interpretation and provided input on the manuscript.

*Address correspondence to: Anne-Lore Schlaitz (a.schlaitz@zmbh.uni-heidelberg.de); Eija Jokitalo (Eija.Jokitalo@Helsinki.fi).

Abbreviations used: aa, amino acid; DSC, dice similarity coefficient; ER, endoplasmic reticulum; FBS, fetal bovine serum; KD, knockdown; MIB, Microscopy Image Browser; NE, nuclear envelope; RHD, reticulon homology domain; RNAi, RNA interference; SB-EM, serial block-face scanning electron microscopy; TEM, transmission electron microscopy.

whether ER overall becomes more tubular or more sheet-like during mitosis is debated. Our earlier work demonstrated that ER undergoes a morphological transition to higher curvature, that is, toward tubules and highly fenestrated sheet remnants, on entry into mitosis (Puhka *et al.*, 2007, 2012). However, others have reported a transition to more cisternal ER during mitosis (Lu *et al.*, 2009; Wang *et al.*, 2013). Importantly, specific factors determining mitotic ER morphology are currently unknown. We previously described REEP3 and REEP4 as RHD proteins that clear ER from metaphase chromosomes in a microtubule-dependent manner (Schlaitz *et al.*, 2013). We now uncover that REEP3/4 induce high curvature ER specifically during mitosis through their RHDs. REEP3/4 may thus molecularly couple membrane shaping and positioning to organize the ER during mitosis. Our findings lend further support to our earlier observations that ER exhibits higher curvature during mitosis than during interphase, assign for the first time a cell cycle-specific function to distinct RHD proteins, and provide a framework for understanding organelle restructuring during mitosis.

RESULTS

REEP3 and REEP4 are required for high ER membrane curvature in mitosis

To identify determinants of mitotic ER morphology, we depleted HeLa cells of selected RHD proteins by RNA interference (RNAi) and analyzed ER structure by confocal light and serial block-face scanning electron microscopy (SB-EM). We chose REEP5 because it is the most abundant RHD protein in HeLa cells (Itzhak *et al.*, 2016; Bekker-Jensen *et al.*, 2017) and REEP3 and REEP4 because of their previously described role in mitotic ER organization (Schlaitz *et al.*, 2013). In control cells, confocal light microscopy showed a diffuse distribution of ER during metaphase. Due to the high density of ER in mitotic cells and the limited resolution of light microscopy, most of the ER signal could not be resolved into individual structures (Figure 1A). Single depletions of REEP3, REEP4, or REEP5 efficiently reduced their respective protein levels but resulted in the same diffuse ER pattern that was observed in control cells (Figure 1, A and B; quantifications in Supplemental Figure S1). REEP3 and REEP4 function redundantly to remove ER from mitotic chromosomes (Schlaitz *et al.*, 2013). We therefore also analyzed REEP3/4 double-depleted cells for ER morphology defects using either a combination of the two single-targeting siRNAs or one double-targeting siRNA. After REEP3/4 double depletion, metaphase ER morphology changed profoundly. Discrete, long curvilinear ER profiles, separated by clearly ER-less regions, were predominant in more than 80% of the cells treated with the double targeting siRNA (Figure 1, A and B, and Supplemental Figure S1). SB-EM analysis revealed that the ER network in control cells was excluded from chromatin and the spindle area. It consisted of many short ER tubules and only a few small or highly fenestrated sheets (Figure 1, C–E; Supplemental Video 1). As these ER structures are small and densely packed (Figure 1E), they appear as diffuse haze by light microscopy (Figure 1A). After REEP3/4 RNAi, large sheets appeared, which were fenestrated to a similar degree as the remaining sheet-like regions in control cells. ER profiles were distributed throughout the entire cell and extended into the spindle area (Figure 1, C–E; Supplemental Video 2). The large and discrete peripheral ER sheets after REEP3/4 RNAi manifest as individual long profiles in cross-section in the confocal light microscopy images (Figure 1A).

For a quantitative analysis of changes in ER morphology, we imaged control, REEP5 RNAi, and REEP3/4 RNAi cells by transmission electron microscopy (TEM) and measured the lengths of peripheral ER profiles in both metaphase and interphase cells. High curvature ER regions such as tubules or small sheets are seen as short profiles, whereas large sheets result in long continuous ER profiles in 60-nm TEM sections. Therefore, the shorter the observed profiles in these analyses, the higher the curvature of the underlying ER morphology (Puhka *et al.*, 2012). In control metaphase cells, 76% of ER profiles had a length between 40 (the shortest expected profile length corresponding to a tubule in cross-section) and 399 nm. Fewer than 4% of the profiles were longer than 1 µm. Upon REEP3/4 RNAi, the length distribution of metaphase ER profiles changed dramatically. Only 29% of REEP3/4 RNAi profiles were between 40 and 399 nm long and more than 40% were longer than 1 µm (Figure 2, A and B). In contrast, ER profile length distributions in interphase were nearly identical for control or REEP3/4-depleted cells (Figure 2, C and D), suggesting that REEP3/4 mediate high curvature of ER specifically during mitosis. Depletion of REEP5 caused no changes in metaphase ER profile lengths (Figure 2, E and F), implying that the total amount of RHD protein was not critical for the observed high curvature ER morphology during mitosis. REEP5 knockdown (KD) did not lead to major changes to interphase ER profile lengths either (Figure 2, G and H), in agreement with previous observations that multiple RHD proteins contribute redundantly to ER morphology in interphase cells (Voeltz *et al.*, 2006; Anderson and Hetzer, 2008). In summary, these results show that REEP3/4 are essential for the normal, high curvature ER morphology during mitosis but are not required for normal interphase ER morphology.

REEP3/4 shape the mitotic ER through their RHD

Next, we tested whether REEP3/4 promote the formation of high curvature ER during mitosis through their RHDs. Since REEP3/4 function redundantly, both in the clearance of ER from chromosomes and in mitotic ER shaping (Schlaitz *et al.*, 2013; Figure 1A), we analyzed REEP4 as a representative for both proteins. We aimed to convert the second hydrophobic hairpin of the REEP4 RHD into a double-spanning transmembrane region by inserting additional hydrophobic residues and replacing two charged amino acids by hydrophobic ones (Figure 3A). Analogous mutations have been shown to abolish the curvature-promoting properties of the RHD of Reticulon 4 (Zurek *et al.*, 2011). We refer to the resulting REEP4 mutant as REEP4(mutRHD) for "REEP4 with mutated RHD." Importantly, REEP4(mutRHD)-HA retained the correct topology because, like wild-type REEP4, it localized to the ER and its C-terminus faced the cytoplasm (Supplemental Figure S2). To examine whether REEP4 and REEP4(mutRHD) could rescue the ER morphology defects after REEP3/4 depletion, we expressed RNAi-resistant versions of the proteins in control and REEP3/4 KD cells containing the general ER marker GFP-Sec61β. Mitotic ER morphology was analyzed in live cells because standard fixation protocols compatible with immunofluorescence staining perturbed mitotic ER morphology. mCherry-tagged Histone 2B (H2B-mCherry) was cotransfected together with the rescue constructs in order to identify transfected cells that expressed the rescue constructs and to label chromatin. In 84% of cells depleted of REEP3/4 and not expressing a rescue construct, the ER was present predominantly in the form of clearly distinguishable long cytoplasmic ER profiles corresponding to large sheets. Wild-type REEP4 largely restored the diffuse ER appearance seen in control cells and corresponding to high curvature ER, whereas REEP4(mutRHD) did not (Figure 3, B and C). Hence, the REEP4 RHD is required to promote tubulation of mitotic ER. REEP4(mutRHD)-HA was present at similar or higher levels than REEP4-HA in the rescue experiments (Figure 3D), excluding the possibility that REEP4(mutRHD) failed to restore ER morphology due to low protein expression.

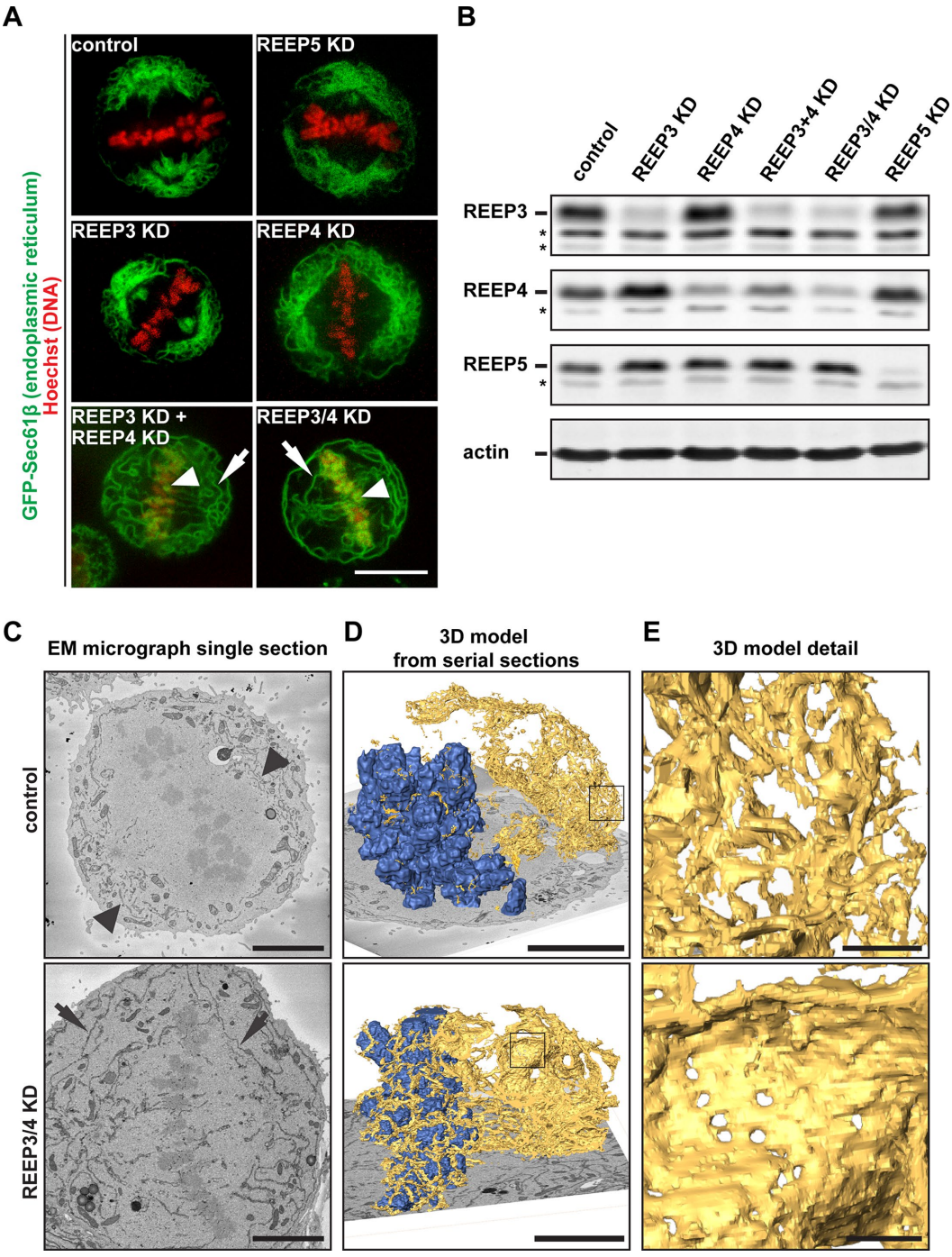

FIGURE 1: Generation of high-curvature ER membranes during mitosis depends on REEP3 and REEP4. (A) HeLa cells stably expressing GFP-Sec61β were transfected with control siRNA; siRNA targeting REEP5, REEP3, or REEP4 individually; a mix of one REEP3- and one REEP4-targeting siRNA; or one single REEP3/4-double targeting siRNA. Cells were imaged live at metaphase. In controls and single depletions, ER had a diffuse overall appearance and remained excluded from chromatin. After REEP3/4 double KD, ER showed long distinct profiles in the cell periphery (arrows) and accumulated on metaphase chromatin (arrowheads). For quantifications, see Supplemental Figure S1. Scale bar is 10 μm. (B) Western blot analysis of KD experiments as shown in panel A confirming efficient depletion of REEP5, REEP3, and REEP4 under the respective conditions. Asterisks indicate nonspecific bands. (C) Single SB-EM images of control and REEP3/4 RNAi cells in metaphase. Control cells show short peripheral ER profiles (arrowheads). In REEP3/4 RNAi cells, ER is present as long profiles in the cell periphery (arrows). Scale bars are 5 μm. (D) A model for chromatin (blue) and ER (yellow) of control and REEP3/4 RNAi cells generated from the SB-EM data set consisting of 550 and 471 block face images, respectively, taken at 30-nm intervals. For clarity, the model displays the ER around chromosomes (ER in up to 320 nm proximity to chromatin) and all ER in a 1.5 μm-wide section across the cell. In control cells, ER exhibits high curvature with tubular and few small sheet regions. In the REEP3/4 RNAi cell, peripheral ER primarily consists of large sheets. For complete models, see Supplemental Videos 1 and 2. Scale bars are 5 μm. (E) Details from the models shown in panel D correspond to the boxed regions. Scale bars are 500 nm.

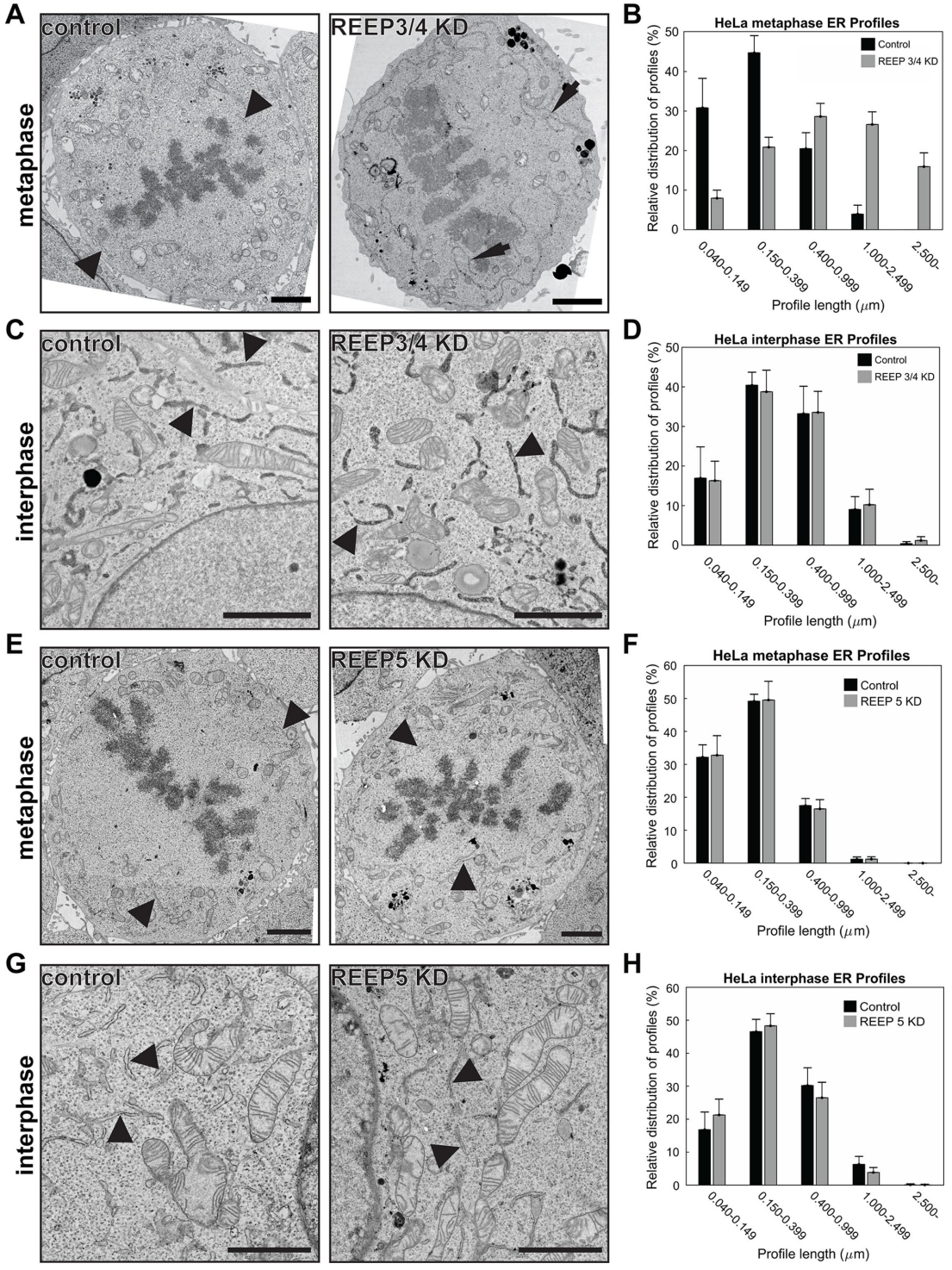

FIGURE 2: Metaphase ER curvature decreases on depletion of REEP3/4. (A) Representative TEM images from metaphase control and REEP3/4 KD cells. (B) Relative distribution of ER profile lengths measured from TEM images of control and REEP3/4 RNAi metaphase cells. Number of cells analyzed; $n = 8$. For a statistical analysis of the difference between the profile length distributions, we determined the DSC, which compares the distribution overlap between two conditions. If the DSC is close to 1, there is a very high overlap between the two distributions; a value of smaller than 1 describes the extent of nonoverlap of the two distributions. For details, see *Materials and Methods*. For metaphase control versus REEP3/4 KD conditions shown in the graph, the DSC is 0.53. (C) As in panel A but with interphase cells. REEP3/4 siRNA and Hsp47-APEX-RDEL were cotransfected. Darker ER staining mediated by Hsp47-APEX-RDEL therefore indicates transfected cells. (D) As in panel B but with interphase cells; $n = 10$. The DSC is 0.98. (E) Representative TEM images from metaphase control and REEP5 KD cells. (F) Relative distribution of ER profile lengths measured from TEM images of control and REEP5 KD metaphase cells; $n = 8$. The DSC is 0.99. (G) As in E but with interphase cells. (H) As in F but with interphase cells; $n = 20$. The DSC is 0.94. (A, C, E, G) Arrowheads and arrows indicate normal and extended profiles, respectively. Scale bars are 2 μm. (B, D, F, H) Data are mean ± SD.

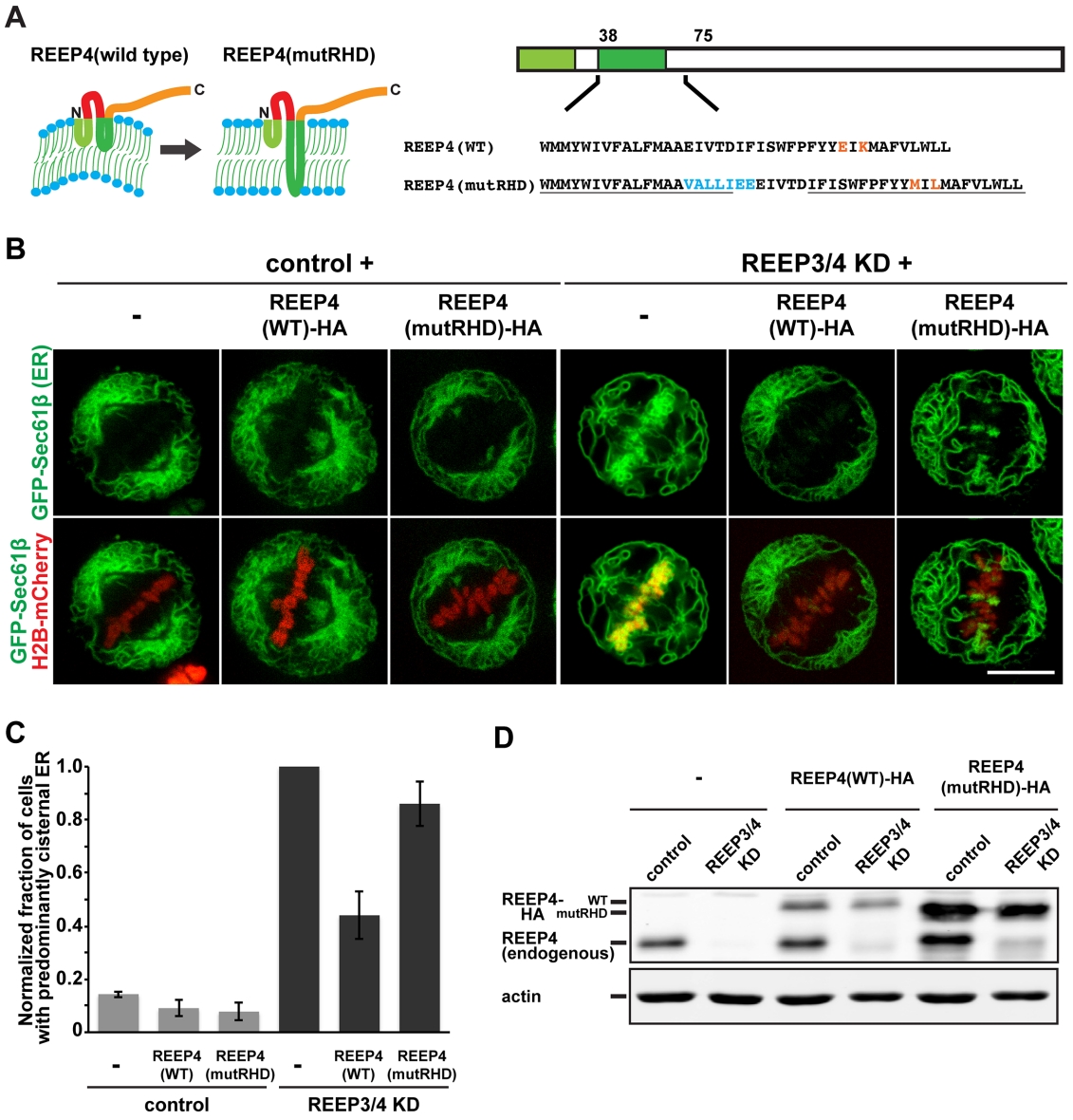

FIGURE 3: Mitotic ER shaping by REEP4 depends on its RHD. (A) Design of a REEP4 RHD mutant. The two putative hairpin regions of the RHD are marked in green. Hypothetical topological models of wild-type REEP4 and REEP4(mutRHD) are on the left; the mutated sequence region is shown on the right. The second hairpin was converted into a double-spanning transmembrane domain in REEP4(mutRHD). Added amino acids are marked in blue, residues mutated from charged to hydrophobic are marked in orange, and the resulting predicted transmembrane segments with lengths of 19 and 21 amino acids are underlined in the displayed sequence. See *Materials and Methods* for details on how the mutant was designed. (B) ER morphology in GFP-Sec61β-expressing control and REEP3/4 KD cells. Cells were cotransfected with H2B-mCherry and either empty HA-tagging plasmid or RNAi-resistant REEP4-HA or REEP4(mutRHD)-HA and imaged live by spinning disk microscopy. Expression of either rescue construct did not affect ER morphology in control cells. REEP4-HA but not REEP4(mutRHD)-HA restored normal ER morphology in metaphase REEP3/4 KD cells. Scale bar is 10 μm. (C) Quantification of mitotic ER morphology phenotypes from data as shown in panel B. Cells with predominantly distinct ER profiles were classified as having abnormal cisternal ER morphology. At least 20 cells were analyzed per condition in each of three independent experiments in a blind way. Results were normalized to the value obtained for nonrescued REEP3/4 KD. REEP3/4RNAi cells expressing either REEP4-HA or REEP4(mutRHD)-HA are significantly different ($p = 0.03$). Statistical testing was done using Welch's *t* test. Error bars are SEM. (D) REEP4(mutRHD)-HA migrates at the expected size in SDS–PAGE and is expressed at higher levels than REEP4-HA in rescue experiments. Cell lysates were generated for the rescue experiment shown in panel B and analyzed by SDS–PAGE and immunoblotting. Endogenous REEP4 as well as REEP4-HA and REEP4(mutRHD)-HA were detected with anti-REEP4 antibody; the same blot was probed for actin as loading control. REEP4(mutRHD)-HA is slightly larger than REEP4-HA but migrates faster in SDS–PAGE, possibly due to a change in hydrophobicity.

Microtubule-dependent clearance of ER from mitotic chromatin requires the cytoplasmic loop of the REEP4 RHD (red in Figure 3A; Schlaitz *et al.*, 2013), which remains intact in REEP4(mutRHD). Accordingly, REEP4 and REEP4(mutRHD) associated with microtubules to a similar extent in a copelleting assay (Figure 4A). To determine whether REEP4(mutRHD) can mediate clearance of ER from

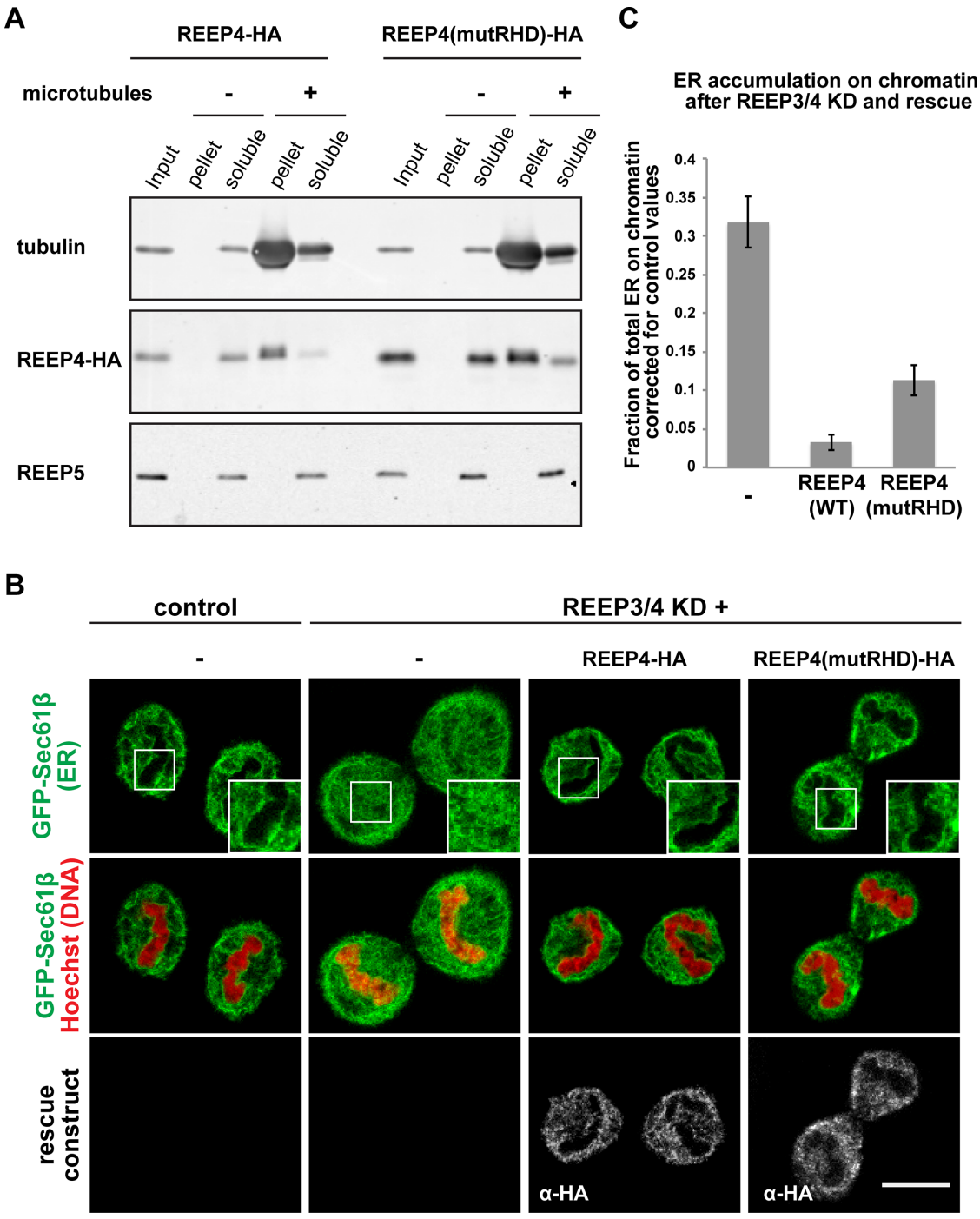

FIGURE 4: ER clearing from chromatin does not require the REEP4 RHD. (A) REEP4-HA and REEP4(mutRHD)-HA were subjected to a microtubule cosedimentation assay. Samples for input, microtubule-bound fraction (pellet), and nonmicrotubule-bound fraction (soluble) were analyzed by SDS–PAGE and immunoblotting. Both REEP4-HA and REEP4(mutRHD)-HA remain soluble in the absence of microtubules but cosediment with taxol-stabilized microtubules. As a negative control, the membrane was probed for REEP5, which remains soluble in the presence of microtubules as previously reported (Schlaitz *et al.*, 2013). (B) Representative confocal images for ER clearing from chromatin in GFP-Sec61β-expressing control or REEP3/4 RNAi cells transfected with plasmids for expression of H2B-mCherry, REEP4-HA, or REEP4(mutRHD)-HA. Immunolabeled HA-tag is shown in gray. Both REEP4 and REEP4(mutRHD) can restore clearing of ER from chromatin in REEP3/4 RNAi cells. Scale bar is 10 μm. (C) Quantification of ER clearing from data as shown in panel B. At least 15 cells undergoing division were analyzed per condition in each of five independent experiments. Shown is the fraction of total ER that associates with chromosomes after REEP3/4 depletion and expression of the different rescue constructs. For each construct, the mean value obtained for ER signal on chromatin after control siRNA treatment (background) was subtracted from the mean value obtained after REEP3/4 siRNA treatment. Values for expression of REEP4-HA or REEP4(mutRHD)-HA are significantly different from H2B-mCherry expression with $p = 0.00056$ and $p = 0.0014$, respectively. Error bars are SEM. Statistical testing was done using Welch's *t* test.

mitotic chromosomes, we analyzed fixed cells with recently segregated chromosomes. GFP-Sec61β expressing HeLa cells were cotransfected with control or REEP3/4 siRNA and either a plasmid encoding H2B-mCherry as a control treatment or with plasmids encoding RNAi-resistant REEP4 or REEP4(mutRHD). ER was excluded from chromatin in cells transfected with control siRNA. In contrast, REEP3/4 depletion caused a strong accumulation of ER on chromatin as expected. Both REEP4 and REEP4(mutRHD) restored clearance of ER from chromatin in REEP3/4 RNAi cells (Figure 4, B and C). REEP4(mutRHD) rescued ER clearance less efficiently than REEP4, possibly because the highly cisternal morphology of the ER in REEP3/4 RNAi cells expressing REEP4(mutRHD) impaired microtubule-based transport of the organelle. Collectively, these results demonstrate that the REEP4 RHD is required for generating high-curvature ER in mitosis but is dispensable for clearing ER from chromatin. Given their high similarity, we assume that the same is true for the REEP3 RHD. Hence, the two functions of REEP3/4 in ER positioning and ER shaping can be uncoupled and the appearance of lower curvature ER after REEP3/4 RNAi is not a consequence of reduced microtubule association of the ER.

The REEP4 C-terminus is required for mitotic ER shaping in addition to the RHD

We next asked how REEP3 and REEP4 are able to shape the ER specifically during mitosis. REEP4 mRNA levels increase during mitosis in Huh-7 cells according to high-throughput data (Palozola *et al.*, 2017). To determine whether REEP3/4 protein levels change during the cell cycle, we collected mitotic cells by shake-off (Schorl and Sedivy, 2007) and compared this mitotically enriched cell population to an interphase-arrested population of cells. REEP4 protein levels were increased by ~50% in the mitotic population, whereas REEP3 protein levels remained nearly unchanged (Supplemental Figure S3). This small difference implied that an adjustment of protein amounts may not be the principal mechanism conferring the mitosis-specific functions of REEP3/4. To determine which regulatory regions of REEP3/4 could be important for their role in mitotic ER shaping, we considered the related REEP1 and REEP2. These two additional members of the REEP1-REEP4 protein family have been shown (for REEP1) or predicted (for REEP2) to associate with microtubules in contrast to the more divergent REEP5/6 proteins (Park *et al.*, 2010; Schlaitz *et al.*, 2013). Both REEP1 and REEP2 are expressed at very low levels in HeLa cells (Bekker-Jensen *et al.*, 2017), consistent with the finding that REEP1 and REEP2 expression cannot be readily detected in non-neuronal tissues (Hurt *et al.*, 2014). REEP1-4 are highly similar in their RHD-containing N-terminal regions but divergent in their C-termini (Park *et al.*, 2010; Supplemental Figure S4). We further investigated REEP2 because REEP1 has a markedly shorter C-terminal region than REEP2, REEP3, or REEP4 (Park *et al.*, 2010; Supplemental Figure S4). Endogenous amounts of REEP2 correspond to ~1% of the combined amounts of endogenous REEP3 and REEP4 based on recent high-throughput proteomics data (Bekker-Jensen *et al.*, 2017). We were not able to detect the REEP2 protein or mRNA in HeLa cells and assumed that any functions of REEP2 in organizing the mitotic ER would likely be compensated for by the much more abundant REEP3/4. We therefore did not attempt to deplete REEP2 from HeLa cells. Instead, we tested whether exogenous expression of REEP2 could rescue the defects of REEP3/4-depletion. REEP2 localized to the ER in interphase and mitotic cells (Supplemental Figure S5) and its overexpression did not perturb ER morphology in control metaphase cells (Supplemental Figure S6). The REEP2 rescue construct was expressed at similar levels as the REEP4 rescue construct in REEP3/4-depleted cells (Figure 5A) but failed to restore high curvature ER morphology during mitosis (Figure 5, B and C). However, REEP2 restored ER clearing from chromosomes in mitotic cells lacking REEP3/4 (Figure 5B). Consistently, REEP2 associated efficiently with microtubules (Supplemental Figure S7). REEP2 thus displays a behavior that is similar to REEP4(mutRHD), despite the fact that the REEP2 N-terminal RHD and surrounding sequences are nearly identical to those of REEP3/4 (Supplemental Figure S4). These observations suggest that REEP3/4 contain residues in their C-terminal regions that promote mitosis-specific ER shaping and may be targets of regulatory inputs. To further test this idea, we created a mutant of REEP4 containing the RHD but lacking the entire C-terminus. We call this N-terminal REEP4 fragment REEP4N (Figure 6A). Additionally, we generated a chimera of REEP2 and REEP4, in which the RHD-containing N-terminus of REEP2 was fused to the C-terminus of REEP4 (REEP2N4C; Figure 6A). REEP4N-HA and REEP2N4C localized to the ER with the predicted topologies (Supplemental Figure S8), were expressed at similar levels as REEP4-HA (Figure 6B), and their exogenous expression did not cause ER morphology defects in control cells (Supplemental Figure S6). Similar to REEP2, REEP4N did not rescue mitotic ER morphology after REEP3/4 depletion (Figure 6, C and D). However, REEP2N4C efficiently restored proper ER morphology in mitotic cells (Figure 6, C and D), suggesting that the putative regulatory sequences derived from REEP4 could now work together with the REEP2 RHD to promote formation of high curvature ER during mitosis.

Thus, the C-terminus of REEP4 harbors residues that are critical for the mitosis-specific functions of the protein. The identification of the signaling mechanisms that govern cell-cycle regulation of REEP3/4 activity will be important tasks for future research.

DISCUSSION

Here we provide new support for our earlier proposal that the ER has a high curvature morphology during mitosis (Puhka *et al.*, 2007, 2012), which had been called into question by Lu *et al.* (2009). We now demonstrate that the RHD proteins REEP3 and REEP4 are important determinants of mitotic ER morphology. We can clearly visualize and distinguish the high curvature morphology of wild-type cells as well as the sheet-like morphology of REEP3/4 RNAi cells, excluding any technical bias in EM sample preparation. REEP3/4 are critical to generate high curvature ER and at the same time position ER away from chromatin during mitosis. REEP3/4 therefore combine distinct molecular activities to create the characteristic organization of the ER during mitosis.

Remarkably, an active RHD within REEP4 and the generation of high curvature peripheral ER are not strictly necessary for the clearing of ER from chromatin. On the other hand, ER morphology during mitosis is not controlled by accumulation of the organelle at the spindle poles as ER morphology remained in an aberrant low curvature state even when positioning was largely normal after rescue with REEP4(mutRHD), REEP2, or the REEP4 truncation mutant REEP4N.

Mitotic ER remodeling is essential in the context of an open mitosis as the NE merges with the peripheral ER on mitotic entry and is reformed from the ER after chromosome segregation. Mitotic NE dynamics and its links to ER organization are still incompletely understood. REEP3/4 as critical ER remodelers will enable the study of how mitotic ER organization impacts NE dynamics. Moreover, the contributions of ER remodeling to the organelle's roles in spindle assembly, chromosome segregation, and cytokinesis can now be addressed.

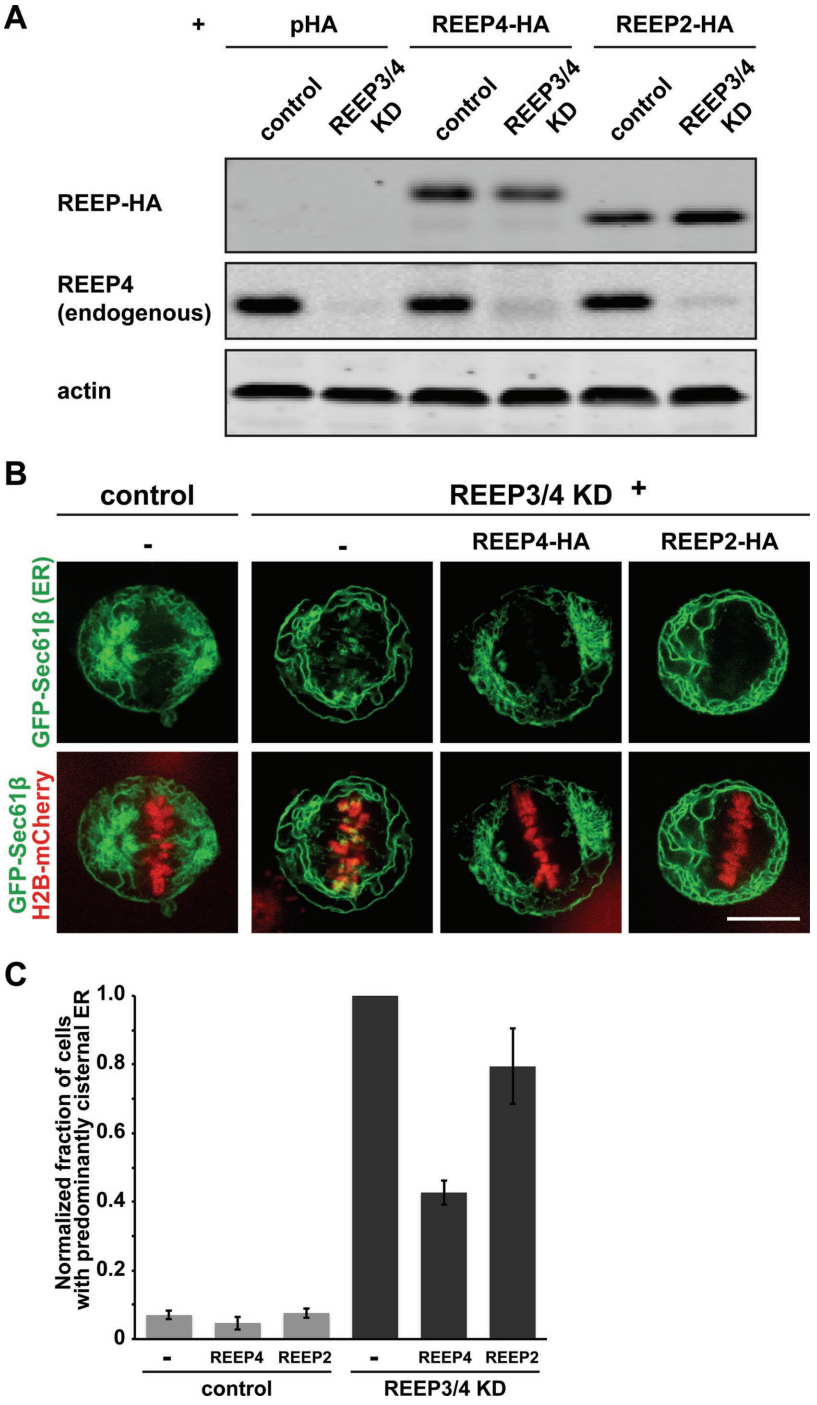

FIGURE 5: Expression of REEP2 does not rescue metaphase ER morphology after REEP3/4 depletion. (A) Cell lysates were generated for the rescue experiments shown in panels B and C and analyzed by SDS–PAGE and immunoblotting. Endogenous REEP4 was detected with anti-REEP4 antibody, HA-tagged constructs were detected with anti-HA antibody, the same membrane was reprobed for actin as loading control. REEP2-HA migrates at the expected size in SDS–PAGE and is expressed at levels comparable to REEP4-HA in rescue experiments. (B) ER morphology in GFP-Sec61β-expressing control and REEP3/4 KD cells. Cells were cotransfected with H2B-mCherry and either empty HA-tagging plasmid or RNAi-resistant REEP4-HA or REEP2-HA and imaged live by spinning disk microscopy. REEP4-HA but not REEP2-HA restored normal ER morphology in metaphase REEP3/4 RNAi cells. Scale bar is 10 μm. (C) Quantification of mitotic ER morphologies from data as shown in panel B. Cells with predominantly distinct ER profiles were classified as having abnormal cisternal ER morphology. At least 20 cells were analyzed per condition in each of four independent experiments. Error bars are SEM. Values for REEP3/4 KD with expression of REEP4-HA versus REEP2-HA are significantly different with $p = 0.04$. Statistical testing was done using Welch's *t* test.

An important question emerging from our study concerns the mitosis-specific regulation of REEP3/4. REEP3/4 protein levels in mitotic versus interphase cells were quite similar. Thus, REEP3/4 activity may be modulated in a cell cycle-specific manner. The observation that the REEP4 C-terminus is required to promote normal high curvature ER morphology during metaphase provides a starting point to identify the signaling pathways that control REEP3/4 functions during mitosis. Insight into the regulation of REEP3/4 may eventually provide a framework to understand the regulation of further ER morphogenic proteins and the mitotic remodeling of other membrane-bound organelles.

In summary, we show that REEP3/4 create high curvature ER during mitosis and have separable functions in mitotic ER shaping and positioning. REEP3/4 provide the first examples of RHD proteins with distinct functions during the cell cycle. Other Reticulon/REEP proteins may similarly have specialized functions, which would begin to explain the puzzling complexity in this group of crucial ER morphogenic proteins.

MATERIALS AND METHODS

Cell culture, siRNAs, plasmids, and transfections

HeLa cells (ATCC CCL-2, authenticated by UC Berkeley tissue culture facility) were cultured in DMEM supplemented with 10% fetal bovine serum (FBS) at 37°C in a humidified 5% CO_2 incubator. HeLa cells stably expressing AcGFP-Sec61β have been described previously (Schlaitz *et al.*, 2013) and were maintained in DMEM/10% FBS supplemented with 400 μg/ml Geneticin (Sigma). Cells were checked for mycoplasma contamination every 6 months and were always negative. For plasmid transfections or siRNA/plasmid cotransfections, 1.8×10^5 cells were seeded in one well of a 24-well plate and transfected the next day with 0.4 μg plasmid DNA using Lipofectamine 2000 (Invitrogen) according to the manufacturer's instructions. siRNAs were transfected using Lipofectamine RNAiMax (Invitrogen) according to the manufacturer's instructions. Three to 6 h after transfection, cells were split onto coverslips or into μ-slide wells (ibidi).

For all rescue experiments, the HA-tagged rescue constructs were cotransfected with H2B-mCherry. All H2B–mCherry-expressing cells were imaged live and considered for analysis. Live cell microscopy had to be performed in order to best preserve ER morphology for assessment of phenotypes. We were not able to express functional fluorescent-protein tagged REEP4 in HeLa cells and therefore had to use the HA-tagged

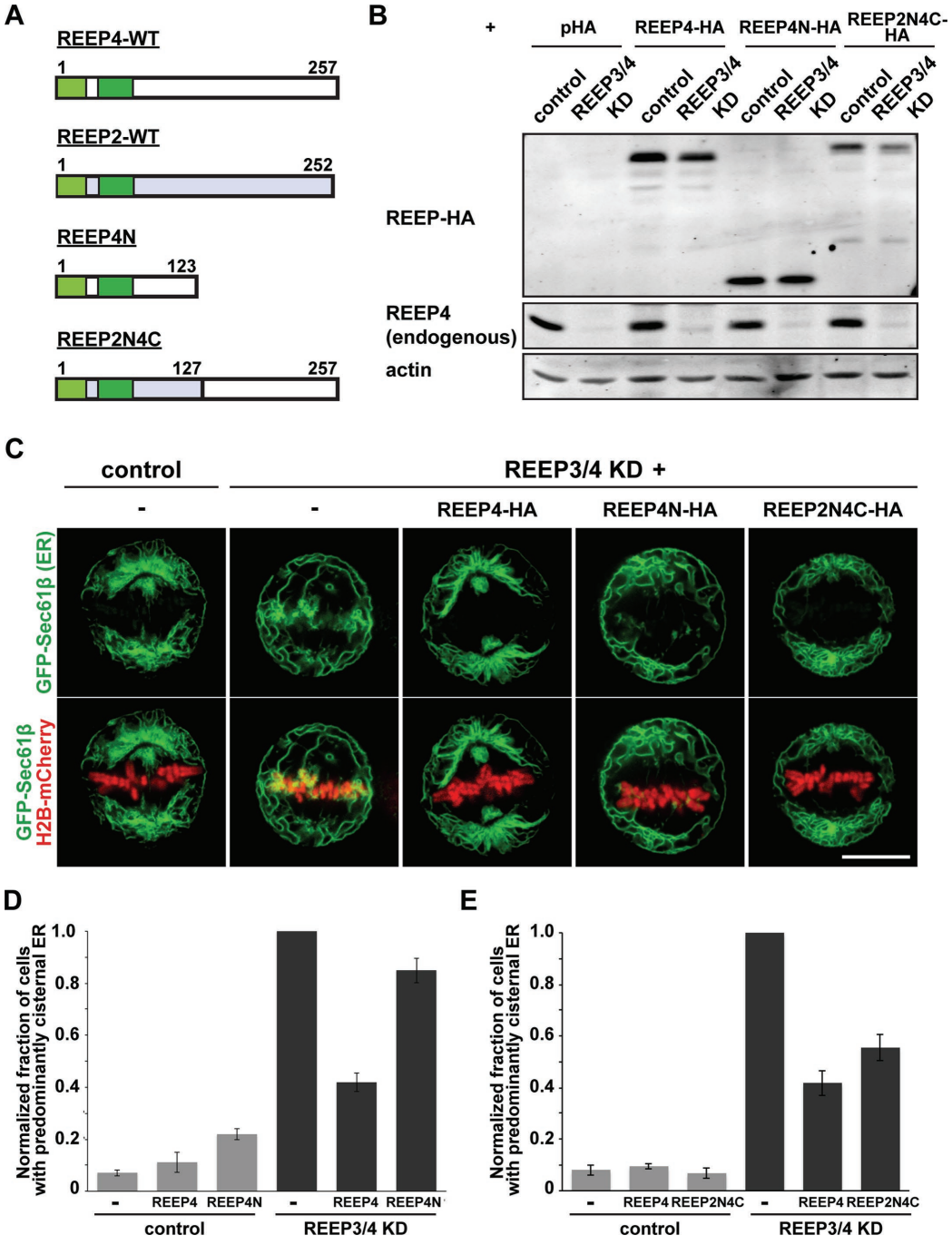

FIGURE 6: Expression of a C-terminal truncation of REEP4 does not rescue metaphase ER morphology after REEP3/4 depletion but REEP2(aa 1–127) fused to a REEP4 C-terminus does. (A) Schematic representation of mutants generated. REEP4N, REEP4 N-terminus (REEP4 aa 1–123); REEP2N4C, chimera consisting of REEP2 aa 1–127 fused to REEP4 aa 128–257. (B) REEP4N-HA and REEP2N4C migrate at the expected size in SDS–PAGE and are expressed at levels comparable to or higher than REEP4-HA in rescue experiments. Cell lysates were generated for the rescue experiments shown in panel C and analyzed by SDS–PAGE and immunoblotting. Endogenous REEP4 was detected with anti-REEP4 antibody, HA-tagged constructs were detected with anti-HA antibody, and the same membrane was probed for actin as loading control. (C) ER morphology in GFP-Sec61β-expressing control and REEP3/4 KD cells. Cells were cotransfected with H2B-mCherry and empty HA-tagging plasmid, or RNAi-resistant REEP4-HA, or REEP4N-HA or REEP2N4C-HA and imaged live by spinning disk microscopy. REEP4-HA and REEP2N4C-HA but not REEP4-N-HA restored normal ER morphology in metaphase REEP3/4 RNAi cells. Scale bar is 10 μm. (D) Quantification of mitotic ER morphologies from data as shown in panel C for rescue with REEP4N. Cells with predominantly distinct ER profiles were classified as having abnormal cisternal ER morphology. At least 20 cells were analyzed per condition in each of five independent experiments. Error bars are SEM. Values for REEP3/4 KD with expression of REEP4-HA versus REEP4N are significantly different with $p = 0.0001$. Statistical testing was done using a *Welch's t test* (E) As in D but for rescue with REEP2N4C. At least 20 cells were analyzed per condition in each of five independent experiments. Error bars are SEM. Values for REEP3/4 KD with expression of REEP4-HA versus REEP2N4C are not significantly different with $p = 0.1$.

Name/catalogue number	Description/reference	Sequence
4392420, s37271 (ThermoFisher)	REEP3/4 double targeting siRNA (Schlaitz *et al.*, 2013)	GGAUUGUUUUUGCACUCUUtt
4392420, s47939 (ThermoFisher)	REEP3 single depletion siRNA (Schlaitz *et al.*, 2013)	CAGUAUGCAUGAUUUAACAtt
AM16708, #32438 (ThermoFisher)	REEP4 single depletion siRNA (Schlaitz *et al.*, 2013)	GGCUGUGAAGACCAAGAACtt
4392420, s15454 (ThermoFisher)	REEP5 siRNA	CGAAGAAAGCUACCGUGAAtt
Ambion negative control, AM4611 siRNA	Nontargeting control siRNA	

TABLE 1: siRNAs used in this study.

constructs that are invisible in our live imaging experiments. However, transfected cells are highly likely to have received both plasmids, H2B-mCherry and the HA-tagged rescue construct (Susa *et al.*, 2008; Xie *et al.*, 2011), and a rescue of ER clearance was observed in the large majority of H2B-mCherry-expressing cells, indicating that they also expressed the rescue constructs. Transfection efficiencies in our experiments were ~ 25%. With this mean transfection efficiency and quantifications of Western blot signal from the lysates of the entire cell populations, we can derive that the rescue constructs in the transfected cells were on average 1.2- to fivefold overexpressed in comparison to endogenous REEP4.

The siRNAs and plasmids used in this study are shown in Tables 1 and 2, respectively.

Rationale for generation of REEP4(mutRHD)-HA. Precise structural information of RHDs is not available but stretches of hydrophobic amino acids within this motif are believed to insert as paired hairpins into the outer leaflet of the ER membrane lipid bilayer, displacing membrane lipids in this leaflet and thus generating or stabilizing high membrane curvature (Voeltz *et al.*, 2006; Hu *et al.*, 2008). An unusual orientation of the membrane-associated segments as well as an amphipathic helix following the RHD have been proposed to contribute to RHD protein function, but the presence of the two hydrophobic RHD hairpins is essential for curvature formation (Brady *et al.*, 2015). Elongation of one or both of the putative RHD hydrophobic hairpins to convert them into double-spanning transmembrane domains has been shown to abolish RHD curvature promoting properties (Zurek *et al.*, 2011). We targeted the second hairpin of REEP4's RHD to preserve the cytoplasmic loop between the hairpins, which is required for microtubule binding. We followed the approach taken by Zurek *et al.* (2011) and inserted five additional hydrophobic amino acids into the first part of the second hairpin to extend this stretch to 19 hydrophobic amino acids, the length of a regular transmembrane span. Immediately following this new transmembrane span, we added two charged glutamate residues. Together with a third glutamate residue already present in

Plasmid name	Description	Source/reference
REEP4(WT)-HA	Human full-length wild-type REEP4, resistant to Ambion siRNA s37271, C-terminally HA-tagged.	Schlaitz *et al.*, 2013
REEP4(mutRHD)-HA	Human full-length REEP4 with mutRHD mutation, resistant to Ambion siRNA s37271, C-terminally HA-tagged.	This study: REEP4-HA was amplified with primers including overhangs coding for the inserted and mutated residues, plasmid was assembled using Gibson assembly (NEB).
H2B-mCherry	Human Histone H2B, C-terminally mCherry-tagged.	Neumann *et al.*, 2010; provided by E. Dultz (ETH Zurich)
Hsp47-APEX-RDEL	Mouse Hsp47 C-terminally tagged with APEX2 and RDEL ER retention signal.	M. Vartiainen (University of Helsinki)
REEP2-HA	Human full-length wild-type REEP2, C-terminally HA-tagged.	This study: REEP2 sequence was PCR amplified from cDNA clone MHS1011-61419 (Open Biosystems) and cloned over *Sac*I/*Sac*II restriction sites into a modified version of pEGFP-N1 (Clontech) in which the pEGFP sequence was replaced by the HA-sequence.
REEP4N-HA	Human REEP4 amino acids 1–123, resistant to Ambion siRNA s37271, C-terminally HA-tagged.	This study: The sequence coding for REEP4 amino acid (aa) 1–123 was PCR amplified from REEP4-HA and cloned over *Sac*I/*Sac*II restriction sites into a modified version of pEGFP-N1 (Clontech) in which the pEGFP sequence was replaced by the HA-sequence.
REEP2N4C-HA	Plasmid expressing a chimeric construct consisting of REEP2(aa1-127) fused to REEP4(aa128–257).	This study: The REEP2-HA plasmid was PCR-linearized excluding the sequence coding for REEP2 aa 128–252. The REEP4 sequence coding for aa 128–257 was amplified from REEP4-HA including overhangs corresponding to the ends of the REEP2-HA PCR product. Both fragments were joined using Gibson assembly (NEB).

TABLE 2: Plasmids used in this study.

Name	Source/reference	Use
Anti-HA-tag 6E2	CST, #2367	immunofluorescence (IF): 1/100
Anti-HA-tag 3F10	Sigma, # 11867423001	Western blotting (WB): 1/5000
Anti-REEP5	Proteintech, 14643-1-AP	WB: 1/5000
Anti-REEP4(7-1)	This study; raised against REEP4 peptide NH2-CDTEAVPRAPARPREK-PLIR-CONH2, position 203-221 of the human REEP4 protein (Pineda Antibody Service).	WB: 1/1000
Anti-REEP3	Abcam, ab106463(Note: major detected band at 35 kDa is background, minor band at around 26 kDa corresponds to REEP3.)	WB: 1/1000
Anti-β-actin	Abcam, ab8224	WB: 1/5000
Anti-phospho-H3 D2C8	CST, #3377T	WB: 1/1000
Anti-GAPDH 14C10	CST, #2118S	WB: 1/1000
Anti-Lamin B1	Abcam, ab 16048	IF: 1/500

TABLE 3: Antibodies used in this study.

the REEP4 sequence, this charged sequence stretch should be forced into the ER lumen. The second part of the predicted hairpin contained many hydrophobic but also polar and charged amino acids. The polar and charged amino acids may affect orientation within the lipid bilayer and thus the functionality of the RHD. To create a morphogenically inert transmembrane span, we mutated two of the charged residues in the second part of the hydrophobic hairpin, generating a second 21 amino acid–long transmembrane segment. According to the transmembrane helices prediction tools TMHMM and TMpred (Hofmann and Stoffel, 1993; Sonnhammer *et al.*, 1998), the mutRHD stretch is highly likely to be a double-spanning transmembrane domain.

Antibodies, immunofluorescence, and light microscopy

For immunofluorescence, cells grown on coverslips were fixed with 3% formaldehyde/0.02% glutaraldehyde (Electron Microscopy Sciences), quenched with 0.5 mg/ml $NaBH_4$ (Sigma), permeabilized with 0.1% Triton X-100 (Merck) in PBS, and blocked with 5% normal donkey serum (Abcam). Primary antibodies were diluted in PBS/0.1% Tween as specified in Table 3. Secondary antibodies were raised in donkey serum, coupled to Alexa 568, Alexa 488, or Alexa 647 dyes (ThermoFisher) and used at a dilution of 1/500. For selective permeabilization of the plasma membrane, coverslips were treated with 40 µg/ml digitonin (Merck) in PBS for 5 min on ice and antibody dilutions were prepared in PBS. DNA was labeled with Hoechst 33342 (Merck). Coverslips were mounted with ProLong Diamond (ThermoFisher) and imaged on a Zeiss LSM780 microscope with a 63× objective using the ZEN software. Live cell imaging was performed on a Leica DMi8 spinning disk microscope using a 63× objective equipped with a Hamamatsu EMCCD camera, Yokogawa spinning disk head, and diode lasers with 488- and 561-nm laser lines. Image acquisition was performed using Metamorph software (Molecular Devices). The microscope was equipped with an environmental chamber. The temperature during live cell imaging was set to 34°C and cells were kept in µ-slides (ibidi) in CO_2-independent L15 medium supplemented with 20% FBS (ThermoFisher).

The antibodies used in this study are shown in Table 3.

Light microscopy image analysis and quantifications

Live microscopy to assess ER morphology under different depletion and rescue conditions. To quantify the occurrence of ER morphology defects, we manually classified the images obtained during live cell microscopy according to the following criteria: ER morphology was considered normal if the majority of peripheral ER displayed a diffuse distribution with at most a few ER-less regions and if only a minor portion of ER was present as curvilinear profiles. ER morphology was considered abnormal (cisternal) if the majority of ER in the periphery was present in the form of long curvilinear profiles with extensive ER-less gaps and if only a minority of ER appeared as a diffuse "haze." Across all experiments and different researchers examining the phenotypes, roughly 80% of cells depleted of REEP3/4 and not expressing a rescue construct displayed abnormal cisternal ER morphology during metaphase.

For the rescue experiments (Figures 3, 5, and 6), we determineed whether the fraction of REEP3/4-depleted cells exhibiting abnormal cisternal ER morphology changed on transfection with the respective rescue constructs (REEP4(WT), REEP4(mutRHD), REEP2, REEP4N, or REEP2N4C) compared with transfection with the empty pHA-vector (nonrescued condition). To exclude a personal bias in the analysis of light microscopy images, we performed a blind classification as follows: individual cells were cropped out from every raw image and saved in the TIF format. Intensities for all color channels across all cropped images were normalized and the resulting images were shuffled and renamed with the experiment date and a randomly assigned number. The shuffled images were independently classified by three of the authors (D.K., B.G., and A.S.) based on the above-mentioned criteria for normal or abnormal ER morphology. Cells for which either of the two phenotypes could not be clearly assigned, usually due to low image quality, were excluded from the analysis. After assigning scoring outcomes back to the individual experimental conditions, the fraction of cells exhibiting abnormal cisternal ER morphology was determined for every experiment and every condition. The obtained fractional values were normalized to the nonrescue condition, that is, REEP3/4 RNAi + pHA. The normalized values were then averaged across the three different scorers and over the different experiments for the respective condition (three to five experiments for every condition, specified in the figure legends), and in the final graphs, the mean of the means of all experiments is shown. The whole workflow was performed using Microscopy Image Browser (MIB) and Matlab (Mathworks, MA). Plot generation and statistics were done with Microsoft Excel.

Sample size was determined by experimental constraints—we acquired as many images of live cells as possible during the 8- to 9-h

imaging sessions. All H2B-mCherry-positive metaphase cells were considered and no cells were excluded at the acquisition stage.

Quantification of ER clearing from chromosomes of fixed telophase cells (Figure 4). Quantification of ER clearing was done using Fiji (Schindelin *et al.*, 2012). Background subtraction was performed using a rolling ball algorithm with a diameter of 150 pixels (corresponding to the average cell size). One mask for chromatin based on Hoechst staining and one mask for the entire cell based on GFP-Sec61β signal were generated, mean intensites of ER signal (GFP-Sec61β) in these two regions were measured, and the ratio between the two values was calculated. Average values obtained for ER mean intensity fraction for control cells were subtracted from the average values obtained for REEP3/4 RNAi cells to visualize the absolute changes in ER accumulation on chromatin.

Microtubule copelleting assays

For microtubule copelleting assays, HEK293T cells were transfected with the respective constructs 48 h before the experiment and lysed by detergent treatment. Lysates were cleared by centrifugation at 10,000 and 100,000 × *g*. The supernatant was supplemented with 1 mM GTP, split in two, and incubated with either buffer or with taxol-stabilized microtubules for 30 min at room temperature. Samples were centrifuged through a sucrose cushion for 30 min at 55,000 × *g* at 25°C. Supernatants and pellets were adjusted to equal volumes and equivalent amounts were analyzed by immunoblotting and detection of tubulin, the HA-tag, or endogenous REEP5.

Electron microscopy and ER profile lengths measurements

For transfections, jetPRIME (Polyplus-transfection, France) or Lipofectamine RNAiMAX (ThermoFisher) were used according to manufacturer's instructions and cells were fixed for analysis 48 h posttransfection (for REEP3/4 depletion) or 72 h posttransfection (REEP5 depletion). For electron microscopy, cells grown on glass coverslips were cytochemically stained and flat embedded as described previously (Jokitalo *et al.*, 2001; Rämö *et al.*, 2016). TEM images were acquired using Jeol JEM-1400 (Jeol, Tokyo, Japan) operating at 80kV equipped with Gatan Orius SC 1000B bottom-mounted CCD-camera (Gatan, Pleasanton, CA).

Samples for SB-EM were prepared as described previously (Puhka *et al.*, 2012). SB-EM data sets were acquired with an FEG-SEM Quanta 250 (ThermoFisher/FEI, Hillsboro, OR) using a back-scattered electron detector (Gatan, Pleasanton, CA) with 2.5-kV beam voltage, a spot size of 3, and a pressure of 0.3 Torr. The block faces were cut with 30-nm increments and imaged with XY resolution of 15 nm per pixel. Image processing and segmentation were done using MIB (Belevich *et al.*, 2016). Visualization of models and rendering of videos were done using Amira (VSG, ThermoFisher/FEI Company).

To measure ER profile lengths in interphase, TEM images from four opposing sides of the nucleus per cell were collected, whereas for the mitotic condition the whole cell was imaged at 2500× magnification. Images from three consecutive sections per cell (n = 8 mitotic or 10 interphase control and REEP3/4 RNAi cells; n = 8 mitotic or 20 interphase control cells for REEP5) were collected. For quantification, a skeleton model of the ER network excluding chromatin associated ER was generated and analyzed using a specially designed plugin in the MIB software.

Statistical analysis of ER profile lengths measurements

The ER profile length analysis (Figure 2) compares the distribution of ER profile lengths over specified categories. A comparative analysis using dice similarity coefficient (DSC) derived from Sørensen's formula was implemented for a statistical evaluation of the profile length distributions in the different KD conditions. A DSC value closer to 1 states a very high overlap or less difference between the two distributions and a DSC value close to 0 relates to a very small overlap between the distributions.

ACKNOWLEDGMENTS

We thank Mervi Lindman (University of Helsinki) for assistance with EM sample preparation, Holger Lorenz (ZMBH) for expert light microscopy support, Helena Bragulat Teixidor (Heidelberg University) for help with mitotic shake-off experiments, and Rebecca Heald (UC Berkeley) and Sebastian Schuck (ZMBH) for discussions and comments on the manuscript. We acknowledge Maria Vartiainen (University of Helsinki) for her kind gift of Hsp47-APEX-RDEL-plasmid. This work was funded by the German Research Foundation (DFG, project no. SCHL1876/2-1, A.S.), the Academy of Finland (project no. 1287975, E.J.), the Sigrid Jusélius Foundation (E.J.), the Biocenter Finland (E.J., and I.B.), and the Helsinki Institute of Life Science Fellow's program (E.J.). D.K. is a graduate student in the program in Integrative Life Science, University of Helsinki. B.G. is a graduate student of the HBIGS Graduate School of Molecular and Cellular Biology of Heidelberg University.

REFERENCES

Anderson DJ, Hetzer MW (2008). Reshaping of the endoplasmic reticulum limits the rate for nuclear envelope formation. J Cell Biol 182, 911–924.

Bekker-Jensen DB, Kelstrup CD, Batth TS, Larsen SC, Haldrup C, Bramsen JB, Sørensen KD, Høyer S, Ørntoft TF, Andersen CL, *et al.* (2017). An optimized shotgun strategy for the rapid generation of comprehensive human proteomes. Cell Systems 4, 587–599.e4.

Belevich I, Joensuu M, Kumar D, Vihinen H, Jokitalo E (2016). Microscopy image browser: a platform for segmentation and analysis of multidimensional datasets. PLoS Biol 14, e1002340.

Brady JP, Claridge JK, Smith PG, Schnell JR (2015). A conserved amphipathic helix is required for membrane tubule formation by Yop1p. Proc Natl Acad Sci USA 112, E639–E648.

Ellenberg J, Siggia ED, Moreira JE, Smith CL, Presley JF, Worman HJ, Lippincott-Schwartz J (1997). Nuclear membrane dynamics and reassembly in living cells: targeting of an inner nuclear membrane protein in interphase and mitosis. J Cell Biol 138, 1193–1206.

Goyal U, Blackstone C (2013). Untangling the web: Mechanisms underlying ER network formation. BBA Mol Cell Res 1833, 2492–2498.

Güttinger S, Laurell E, Kutay U (2009). Orchestrating nuclear envelope disassembly and reassembly during mitosis. Nat Rev Mol Cell Biol 10, 178–191.

Hofmann K, Stoffel W (1993). TMBASE—a database of membrane spanning protein segments. Biol Chem Hoppe-Seyler 374, 166.

Hu J, Shibata Y, Voss C, Shemesh T, Li Z, Coughlin M, Kozlov MM, Rapoport TA, Prinz WA (2008). Membrane proteins of the endoplasmic reticulum induce high-curvature tubules. Science 319, 1247–1250.

Hurt CM, Björk S, Ho VK, Gilsbach R, Hein L, Angelotti T (2014). REEP1 and REEP2 proteins are preferentially expressed in neuronal and neuronal-like exocytotic tissues. Brain Res 1545, 12–22.

Itzhak DN, Tyanova S, Cox J, Borner GH (2016). Global, quantitative and dynamic mapping of protein subcellular localization. Elife 5, 570.

Jokitalo E, Cabrera-Poch N, Warren G, Shima DT (2001). Golgi clusters and vesicles mediate mitotic inheritance independently of the endoplasmic reticulum. J Cell Biol 154, 317–330.

Lu L, Ladinsky MS, Kirchhausen T (2009). Cisternal organization of the endoplasmic reticulum during mitosis. Mol Biol Cell 20, 3471–3480.

Neumann B, Walter T, Hériché JK, Bulkescher J, Erfle H, Conrad C, Rogers P, Poser I, Held M, Liebel U, *et al.* (2010). Phenotypic profiling of the human genome by time-lapse microscopy reveals cell division genes. Nature 464, 721–727.

Palozola KC, Donahue G, Liu H, Grant GR, Becker JS, Cote A, Yu H, Raj A, Zaret KS (2017). Mitotic transcription and waves of gene reactivation during mitotic exit. Science 358, 119–122.

Park SH, Zhu P-P, Parker RL, Blackstone C (2010). Hereditary spastic paraplegia proteins REEP1, spastin, and atlastin-1 coordinate microtubule interactions with the tubular ER network. J Clin Invest 120, 1097–1110.
Prekeris R, Gould GW (2008). Breaking up is hard to do—membrane traffic in cytokinesis. J Cell Sci 121, 1569–1576.
Puhka M, Joensuu M, Vihinen H, Belevich I, Jokitalo E (2012). Progressive sheet-to-tubule transformation is a general mechanism for endoplasmic reticulum partitioning in dividing mammalian cells. Mol Biol Cell 23, 2424–2432.
Puhka M, Vihinen H, Joensuu M, Jokitalo E (2007). Endoplasmic reticulum remains continuous and undergoes sheet-to-tubule transformation during cell division in mammalian cells. J Cell Biol 179, 895–909.
Rämö O, Kumar D, Gucciardo E, Joensuu M, Saarekas M, Vihinen H, Belevich I, Smolander OP, Qian K, Auvinen P, *et al*. (2016). NOGO-A/RTN4A and NOGO-B/RTN4B are simultaneously expressed in epithelial, fibroblast and neuronal cells and maintain ER morphology. Sci Rep 6, 1–14.
Schellhaus AK, De Magistris P, Antonin W (2016). Nuclear reformation at the end of mitosis. J Mol Biol 428, 1962–1985.
Schindelin J, Arganda-Carreras I, Frise E, Kaynig V, Longair M, Pietzsch T, Preibisch S, Rueden C, Saalfeld S, Schmid B, *et al*. (2012). Fiji: an open-source platform for biological-image analysis. Nat Methods 9, 676–682.
Schlaitz A-L, Thompson J, Wong CCL, Yates JR III, Heald R (2013). REEP3/4 Ensure endoplasmic reticulum clearance from metaphase chromatin and proper nuclear envelope architecture. Dev Cell 26, 315–323.
Schorl C, Sedivy JM (2007). Analysis of cell cycle phases and progression in cultured mammalian cells. Methods 41, 143–150.
Schweizer N, Pawar N, Weiss M, Maiato H (2015). An organelle-exclusion envelope assists mitosis and underlies distinct molecular crowding in the spindle region. J Cell Biol 210, 695–704.
Shibata Y, Shemesh T, Prinz WA, Palazzo AF, Kozlov MM, Rapoport TA (2010). Mechanisms determining the morphology of the peripheral ER. Cell 143, 774–788.
Shibata Y, Voeltz GK, Rapoport TA (2006). Rough sheets and smooth tubules. Cell 126, 435–439.
Sonnhammer EL, von Heijne G, Krogh A. (1998). A hidden Markov model for predicting transmembrane helices in protein sequences. Proc Int Conf Intell Syst Mol Biol 6, 175–182.
Susa T, Kato T, Kato Y (2008). Reproducible transfection in the presence of carrier DNA using FuGENE6 and Lipofectamine2000. Mol Biol Rep 35, 313–319.
Voeltz GK, Prinz WA, Shibata Y, Rist JM, Rapoport TA (2006). A class of membrane proteins shaping the tubular endoplasmic reticulum. Cell 124, 573–586.
Wang S, Romano FB, Field CM, Mitchison TJ, Rapoport TA (2013). Multiple mechanisms determine ER network morphology during the cell cycle in Xenopus egg extracts. J Cell Biol 203, 801–814.
Westrate LM, Lee JE, Prinz WA, Voeltz GK (2015). Form follows function: the importance of endoplasmic reticulum shape. Annu Rev Biochem 84, 791–811.
Xie ZL, Shao SL, Lv JW, Wang CH, Yuan CZ, Zhang WW, Xu XJ (2011). Co-transfection and tandem transfection of HEK293A cells for overexpression and RNAi experiments. Cell Biol Int 35, 187–192.
Zhang D, Vjestica A, Oliferenko S (2010). The Cortical ER network limits the permissive zone for actomyosin ring assembly. Curr Biol 20, 1029–1034.
Zurek N, Sparks L, Voeltz G (2011). Reticulon short hairpin transmembrane domains are used to shape ER tubules. Traffic 12, 28–41.